NACA

RESEARCH MEMORANDUM

THE EFFECT OF NACELLE LOCATION ON THE ZERO-LIFT DRAGS OF 45° SWEPTBACK WING-BODY CONFIGURATIONS HAVING BOATTAIL AND CYLINDRICAL AFTERBODIES AS DETERMINED BY FLIGHT TESTS AT TRANSONIC SPEEDS

By Sherwood Hoffman and Austin L. Wolff

Langley Aeronautical Laboratory
Langley Field, Va.

NATIONAL ADVISORY COMMITTEE
FOR AERONAUTICS

WASHINGTON
March 25, 1954

NATIONAL ADVISORY COMMITTEE FOR AERONAUTICS

RESEARCH MEMORANDUM

THE EFFECT OF NACELLE LOCATION ON THE ZERO-LIFT DRAGS OF 45° SWEPTBACK WING-BODY CONFIGURATIONS HAVING BOATTAIL AND CYLINDRICAL AFTERBODIES AS DETERMINED BY FLIGHT TESTS AT TRANSONIC SPEEDS

By Sherwood Hoffman and Austin L. Wolff

SUMMARY

The effects of nacelle location on the zero-lift drags of 45° swept-back wing-body combinations having boattail and cylindrical afterbodies have been determined by flight tests of rocket-propelled models through a range of Mach numbers from 0.8 to 1.25 and Reynolds numbers from 4×10^6 to 7×10^6 based on the wing mean aerodynamic chord. The nacelles were tested at the wing root, at 40 percent of the semispan, and at the wing tips. The effect of afterbody shape was investigated by replacing the boattail afterbody of the fuselage with a cylinder.

The trends in drag rises and nacelle-plus-interference drag coefficients of the models were found to be in qualitative agreement with the concepts of the transonic area rule near Mach number 1.0. Favorable interference effects were obtained from the wing-tip nacelles throughout the test range regardless of the afterbody shape used. The nacelles at the wing root and at 40 percent of the semispan experienced unfavorable interference effects near Mach number 1.0. Changing from the boattail afterbody to the cylindrical afterbody resulted in a general reduction in the pressure drag (base drag excluded) of all the configurations, except for the model with the wing-tip nacelles, near and above Mach number 1.0. This change in afterbody shape also reduced the unfavorable interference from the nacelles at the wing root and the 40-percent-semispan station near the speed of sound. A large part of the interference effects was due to wing-nacelle interference. The drag-rise Mach numbers varied between 0.92 and 0.96, the highest drag-rise Mach numbers being obtained from the models without nacelles.

INTRODUCTION

As part of a general transonic research program of the National Advisory Committee for Aeronautics to investigate the aerodynamic characteristics of promising aircraft configurations, the Langley Pilotless Aircraft Research Division (at its testing station at Wallops Island, Va.) has tested a series of rocket-propelled free-flight models to determine the effect of nacelle location on the zero-lift drags of high-aspect-ratio, 45° sweptback wing-body combinations. Previous investigations (refs. 1 to 8) have shown that large changes in interference effects are obtained near Mach number 1.0 when the nacelle position is varied spanwise, chordwise, or vertically and when various nacelle sizes or combinations are used on the wing of a configuration that had a fuselage with a boattail afterbody. The present paper shows the effect of changing the fuselage afterbody shape on the drag of the configuration and on the interference drags of three of the spanwise nacelle positions tested at transonic speeds. The boattail afterbody of the original fuselage was replaced by a long cylinder; thus, the fuselage fineness ratio was increased from 10 to about 12. Cross-sectional area diagrams are presented for the wing-body-nacelle models having the cylindrical afterbody and boattail afterbody in order to compare the drag rises of the models according to the concepts of the transonic area rule (ref. 9).

Solid nacelles were located at the wing tips, at 40 percent of the semispan, and at the wing root for the present tests. The nacelles were made solid by fairing the NACA 1-50-250 nose inlet to a point, in order to simplify the construction.

Flight tests covered a continuous range of Mach number varying between 0.8 and 1.25 with corresponding Reynolds numbers from 4×10^6 to 7×10^6 based on wing mean aerodynamic chord.

SYMBOLS

A	cross-sectional area, ft^2
a	tangential acceleration, ft/sec^2
b	wing span, ft
C_D	drag coefficient, $C_{D_T} - C_{D_B} - C_{D_{fins}}$, based on S_w
C_{D_B}	base drag coefficient, based on S_w

$C_{D_{fins}}$	fin drag coefficient, based on S_w
C_{D_N}	nacelle-plus-interference drag coefficient, based on total nacelle frontal area
C_{D_T}	total drag coefficient, based on S_w
c	wing chord, ft
g	acceleration due to gravity, 32.2 ft/sec^2
l_f	length of original body, ft
M	Mach number
p_B	base pressure, lb/ft^2
p	free-stream static pressure, lb/ft^2
q	free-stream dynamic pressure, lb/ft^2
R	Reynolds number, based on mean aerodynamic chord
r_{eq}	radius of equivalent body of revolution, ft
S_B	base area of fuselage, ft^2
S_N	frontal area of one nacelle, ft^2
S_w	total plan-form area of wing, ft^2
w	weight of model during deceleration, lb
θ	angle between flight path and horizontal, deg
x	longitudinal station
y	airfoil ordinate

MODELS

Details and dimensions of the basic wing-body configurations having the cylindrical body and the original body (ref. 2) are given in figure 1

and tables I to III. Dimensions of the nacelle are given in figure 2 and table IV. Photographs of the models and diagrams showing the nacelle locations, equivalent bodies of revolution, and cross-sectional area distribution of the models are presented in figures 3 and 4. The cross-sectional area of the stabilizing fins is not included in the area diagrams.

The cylindrical-body-plus-wing configuration was similar to the original basic configuration used in previous investigations (refs. 1 to 8) except for the shape of the fuselage afterbody. The boattail afterbody of the original fuselage was replaced by a long cylinder behind the maximum diameter station (fig. 1) that increased the fuselage fineness ratio from 10.0 to 11.95. The wing had a sweepback angle of 45° along the quarter-chord line, an aspect ratio of 6.0 (based on total wing plan-form area), a taper ratio of 0.6, and an NACA 65A009 airfoil section in the free-stream direction. The ratio of total wing-plan-form area to fuselage frontal area was 16.0. Two vertical fins were used to stabilize the model directionally. No fins were required in the horizontal plane because the sweptback wing was located far enough rearward to stabilize the model longitudinally.

Each nacelle was a solid body of revolution (fig. 2) having a nose plug, an NACA 1-50-250 nose-inlet profile, a cylindrical midsection, and an afterbody with the proportions of form 111 (ref. 2). The fineness ratio of the solid nacelle was 9.66. The nacelles were symmetrically mounted on the wing and were tested in three spanwise positions (fig. 3) measured from the fuselage center line. The chordwise positions of the nacelles, measured between the nacelle nose and wing maximum thickness (0.4c), was kept constant at a length equal to 116 percent of the wing mean aerodynamic chord. For convenience, a list of the models tested and their identifying symbols is presented in the following table:

Model	Fuselage or body	Nacelle spanwise location, percent b/2
A	Cylindrical	----------
B	Cylindrical	96 (wing tip)
C	Cylindrical	40
D	Cylindrical	15 (wing root)
E	Original (ref. 2)	----------
F	Original (ref. 1)	96 (wing tip)
G	Original (ref. 1)	40
H	Original (ref. 7)	15 (wing root)

An NACA two-channel telemeter for transmitting longitudinal accelerations and base pressures was installed in the nose of models A and E.

The base pressures on model A were obtained from eight manifolded orifices (0.05-inch diameter) equally spaced on a tubular ring located at the base as is shown in figure 1. This arrangement provided a more accurate determination of the average base pressures than was obtained from the single base pressure orifice (fig. 1), 65° from the wing plane, on model E.

TESTS AND MEASUREMENTS

The rocket-propelled zero-lift models were tested at the Langley Pilotless Aircraft Research Station at Wallops Island, Va. Each model was propelled by a two-stage rocket system and launched from a rail launcher (fig. 5). The first stage consisted of a 5-inch lightweight high-velocity aircraft rocket motor that served to accelerate the model to high subsonic speeds. For the second stage, a 3.25-inch Mark 7 aircraft rocket motor was installed in the fuselage to accelerate the model to supersonic speeds. Tracking instrumentation consisting of a CW Doppler velocimeter and an NACA modified SCR-584 tracking unit were used to determine the velocity, deceleration, and flight path of all the models during coasting flight. The two-channel telemeter installed in the nose of the basic wing-body configurations transmitted a continuous record of base pressures and longitudinal accelerations from the models to a ground receiving station. A survey of atmospheric conditions was made by radiosonde measurements from an ascending balloon that was released at the time of each launching.

The flight tests covered a continuous range of Mach number varying between 0.8 and 1.25. The corresponding Reynolds numbers varied from approximately 4×10^6 to 7×10^6 based on wing mean aerodynamic chord as is shown in figure 6.

The values of total drag coefficient and base drag coefficient, based on total wing plan-form area, were obtained with the following expressions:

$$C_{D_T} = -\frac{W}{gqS_w}(a + g \sin \theta)$$

$$C_{D_B} = \left(\frac{p_B - p}{q}\right)\frac{S_B}{S_w}$$

The total drag coefficients for the original models with the boattail afterbody were obtained from references 1 and 7. The base drag for the original wing-body was not given in reference 2 and is presented herein.

The base drag coefficients of the models with nacelles were assumed to be the same as C_{D_B} measured on the corresponding wing-body models on the premise that the nacelles would have little or no effect on the base drags.

The drag coefficients of the configurations were obtained by subtracting the base drag and fin drag coefficients from the total drag coefficients as follows:

$$C_D = C_{D_T} - C_{D_B} - C_{D_{fins}}$$

where $C_{D_{fins}}$ is based on S_W. The drag of the fins plus interference was established from previous flight tests of models that had twice-scale fins mounted as wings on a cylindrical fuselage and is shown in figure 7. Estimates indicate that the fin-plus-interference drag coefficients would not be changed by adding the wings and nacelles in the manner employed on the test models.

The nacelle-plus-interference drag coefficients were obtained by subtracting the drags of the models without nacelles from the drags of the corresponding models with nacelles. This coefficient, based on total nacelle frontal area, is expressed by

$$C_{D_N} = \left(C_{D_{\text{nacelles on}}} - C_{D_{\text{nacelles off}}}\right)\frac{S_W}{2S_N}$$

Values of C_{D_N} less than that of the isolated nacelle (ref. 8) represent the presence of favorable interference effects.

When the present data were reduced, the probable errors in total drag coefficient were determined from comparisons of C_{D_T} as determined from accelerations measured by the accelerometers in models A and E and accelerations obtained from differentiating the velocity-time curves of the CW Doppler velocimeter. The true airspeeds of the models were obtained by correcting the CW Doppler velocity measurements for winds aloft; thus, the errors in M and q were minimized. The measurements of base pressure and atmospheric pressure were accurate to about 0.07 lb/sq in. From these considerations, the probable errors in the measured drag coefficients are believed to be as follows:

$C_{D_T}(0.8 < M < 1.05)$ . . . . . ±0.0010
$C_{D_T}(1.05 < M < 1.25)$ . . . . . ±0.0005
$C_{D_B}(0.8 < M < 1.05)$ . . . . . ±0.0020
$C_{D_B}(1.05 < M < 1.25)$ . . . . . ±0.0008
$M(0.8 < M < 1.25)$ . . . . . ±0.005

RESULTS AND DISCUSSION

Faired curves showing the variations of total drag, base drag, and fin drag coefficients with Mach number for the models with the cylindrical body and with the original boattail body are given in figures 7(a) and 7(b). The effect of nacelle location and afterbody shape on the drag through the Mach number range is presented in figures 8 and 9. The nacelle-plus-interference drag coefficients are compared in figure 10. The drag of the isolated nacelles shown in figures 8 and 10 were obtained in an earlier investigation (ref. 8).

The results in figures 8(a) and 8(b) show that mounting the nacelles at the wing root or at the 40-percent-semispan station resulted in the largest incremental drags near Mach number 1.0 and to the upper limits of the tests on either the cylindrical body or original boattail body configurations. A comparison of these drag increments with the drag from the isolated nacelles in figure 8 shows that the interference effects were greater from the nacelles on the boattail body models than from the nacelles on the corresponding cylindrical body models near the speed of sound. Above Mach number 1.05, the total spread between the curves in figures 8(a) and 8(b) are of the same order of magnitude and indicates that a large part of the interference effects were due to wing-nacelle interference. The relatively small changes in drag obtained when the nacelles were mounted at the wing tips resulted from favorable interference throughout the Mach number range.

The variations of C_D with M in figure 9 show that replacing the boattail afterbody with the cylindrical afterbody reduced the drag coefficient of the basic configuration (model E) by about 0.0035 above Mach number 1.0. The changes in drag coefficient obtained for the configurations with nacelles were less, greater, or of the same order of magnitude as that from the basic configuration; thus, the interference effects changed when the boattail afterbody was replaced by the cylindrical afterbody. The change in interference effects with afterbody shape may be seen more clearly from the comparisons of the nacelle-plus-interference drag coefficients in figure 10.

The favorable interference effects obtained from the wing-tip nacelles were reduced throughout the test range when the cylindrical afterbody configuration was used. For the nacelles located at the 15-percent- and 40-percent-semispan stations, changing from the boattail afterbody to the cylindrical afterbody decreased the unfavorable interference near the speed of sound and increased the interference drag at the higher Mach numbers of the test range.

The transonic area rule (ref. 9) provides a simple basis for explaining the drag rises of aircraft configurations near Mach number 1.0. This rule states that the zero-lift drag rise of thin, low-aspect-ratio wing-body combinations near the speed of sound is primarily dependent on the axial distribution of the cross-sectional areas of the configuration normal to the axis of symmetry. Recent investigations (refs. 8, 10, 11, 12) have shown that the area rule may be used to compare the drag rises of configurations having nacelles or external stores on wings of moderate aspect ratios to a limited extent. References 8 and 12 indicate that the drag rises of such configurations can be explained (1) by comparing the total cross-sectional area distributions of the configurations and (2) by comparing the displacements between the nacelle peak area and the maximum area of the basic configuration resulting from changing the nacelle location. In this paper, the cross-sectional area distributions of the models are presented in figure 4 for comparison with the drag rises in figures 8 and 9.

When the nacelle positions are varied spanwise, as on the configurations with the cylindrical body (models A to D), there is a noticeable change in the cross-sectional areas and drag rises of the models, as is shown in figures 4 and 8(a). The highest drag rise was obtained from the nacelle positions (models C and D) giving the largest maximum cross-sectional areas, which gave the smallest displacement between the peak areas of the nacelles and the basic configuration and highest slopes before and after the peak area position. Figures 8(b) and 4 show that this same effect was obtained when the nacelles were varied spanwise on the models with the boattail afterbody (models E to H). By changing from the boattail afterbody to the longer cylindrical afterbody, the peak areas were increased slightly and the slopes reduced for the basic configuration without nacelles and with the nacelles located at the 15-percent- and 40-percent-semispan stations. The slight increase in maximum area was not great enough to offset the gains from the lower slopes; consequently, the drag rises were reduced. For the models with the wing-tip nacelles, this change in afterbody shape increased the maximum area enough to offset the gain obtained from the reduced slopes and had no apparent effect on the drag rise of the configuration.

Previous investigations (for example, ref. 4) and model F show that the drag of the boattail configuration is reduced near Mach number 1.0 due to extremely favorable interference when the nacelles are added to

the wing tips. The present tests offer a possible explanation for this extremely favorable interference. When the nacelles are mounted on the wing tips, the shock wave off the base of the boattail afterbody intersects the rearward part of the nacelle and induces positive pressures to lower the drag. By changing to the longer cylindrical afterbody, the shock wave from the base was moved rearward and did not intersect the wing-tip nacelle. As a consequence, there was a noticeable reduction in the favorable interference at the wing tips as is shown in figure 10(a).

The drag-rise Mach numbers of all the configurations tested varied between 0.92 and 0.96, the highest drag-rise Mach number being obtained for the basic wing-body configurations without nacelles.

CONCLUSIONS

The effects of nacelle location and afterbody shape on the zero-lift drag of a 45° sweptback wing-body configuration have been determined by flight tests between Mach number 0.8 and 1.25. The nacelles were tested at the wing root, at 40 percent of the semispan, and at the wing tips. The effect of afterbody shape was investigated by replacing the boattail afterbody with a cylinder. The results indicate the following:

1. The trends in drag rises and nacelle-plus-interference drag coefficients near Mach number 1.0 were found to be in qualitative agreement with the concepts of the transonic area rule.

2. Favorable interference effects were obtained from the wing-tip nacelles throughout the Mach number range regardless of the afterbody shape used. The nacelles at the wing root and at 40 percent of the semispan experienced unfavorable interference effects near Mach number 1.0.

3. Changing from the boattail afterbody to the cylinder on the configurations tested resulted in a general reduction in the pressure drag (base drag excluded), of all the models, except for the configuration with the wing-tip nacelles, near and above Mach number 1.0. This change in afterbody shape reduced the unfavorable interference from the nacelles at the wing root and the 40-percent-semispan station near Mach number 1.0.

4. A large part of the interference effects was due to wing-nacelle interference.

5. The drag rise Mach numbers varied between 0.92 and 0.96, the highest drag rise Mach numbers being obtained from the models without nacelles.

Langley Aeronautical Laboratory,
National Advisory Committee for Aeronautics,
Langley Field, Va., January 20, 1954.

REFERENCES

1. Pepper, William B., Jr., and Hoffman, Sherwood: Comparison of Zero-Lift Drags Determined by Flight Tests at Transonic Speeds of Symmetrically Mounted Nacelles in Various Spanwise Positions on a 45° Sweptback Wing and Body Combination. NACA RM L51D06, 1951.

2. Pepper, William B., Jr., and Hoffman, Sherwood: Transonic Flight Tests To Compare the Zero-Lift Drag of Underslung and Symmetrical Nacelles Varied Chordwise at 40 Percent Semispan of a 45° Sweptback, Tapered Wing. NACA RM L50G17a, 1950.

3. Hoffman, Sherwood: Transonic Flight Tests To Compare the Zero-Lift Drags of Underslung Nacelles Varied Spanwise on a 45° Sweptback Wing and Body Combination. NACA RM L52D04a, 1952.

4. Pepper, William B., Jr., and Hoffman, Sherwood: Comparison of Zero-Lift Drags Determined by Flight Tests at Transonic Speeds of Symmetrically Mounted Nacelles in Various Chordwise Positions at the Wing Tip of a 45° Sweptback Wing and Body Combination. NACA RM L51F13, 1951.

5. Hoffman, Sherwood, and Mapp, Richard C., Jr.: Transonic Flight Tests To Compare the Zero-Lift Drags of 45° Sweptback Wings of Aspect Ratio 3.55 and 6.0 With and Without Nacelles at the Wing Tips. NACA RM L51L27, 1952.

6. Hoffman, Sherwood, and Pepper, William B., Jr.: Transonic Flight Tests To Determine Zero-Lift Drag and Pressure Recovery of Nacelles Located at the Wing Tips on a 45° Sweptback Wing and Body Combination. NACA RM L51K02, 1952.

7. Hoffman, Sherwood, and Wolff, Austin L.: Transonic Flight Tests To Determine Zero-Lift Drag and Pressure Recovery of Nacelles Located at the Wing Root on a 45° Sweptback Wing and Body Configuration. NACA RM L53H20, 1953.

8. Hoffman, Sherwood, and Pepper, William B., Jr.: The Effect of Nacelle Combinations and Size on the Zero-Lift Drag of a 45° Sweptback Wing and Body Configuration as Determined by Free-Flight Tests at Mach Numbers Between 0.8 and 1.3. NACA RM L53E25, 1953.

9. Whitcomb, Richard T.: A Study of the Zero-Lift Drag-Rise Characteristics of Wing-Body Combinations Near the Speed of Sound. NACA RM L52H08, 1952.

10. Whitcomb, Richard T.: Recent Results Pertaining to the Application of the "Area Rule." NACA RM L53I15a, 1953.

11. Hall, James Rudyard: Comparison of Free-Flight Measurements of the Zero-Lift Drag Rise of Six Airplane Configurations and Their Equivalent Bodies of Revolution at Transonic Speeds. NACA RM L53J21a, 1953.

12. Smith, Norman F., Bielat, Ralph P., and Guy, Lawrence D.: Drag of External Stores and Nacelles at Transonic and Supersonic Speeds. NACA RM L53I23b, 1953.

TABLE I.- COORDINATES OF CYLINDRICAL FUSELAGE

[Station measured from fuselage nose]

Station, in.	Ordinate, in.
0	0
.4	.185
.6	.238
1.0	.342
2.0	.578
4.0	.964
6.0	1.290
8.0	1.577
12.0	2.074
16.0	2.472
20.0	2.772
24.0	2.993
28.0	3.146
32.0	3.250
36.0	3.314
40.0	3.334
79.7	3.334

TABLE II.- COORDINATES OF ORIGINAL FUSELAGE[1]

Station measured from fuselage nose

Station, in.	Ordinate, in.
0	0
.4	.185
.6	.238
1.0	.342
2.0	.578
4.0	.964
6.0	1.290
8.0	1.577
12.0	2.074
16.0	2.472
20.0	2.772
24.0	2.993
28.0	3.146
32.0	3.250
36.0	3.314
40.0	3.334
44.0	3.304
48.0	3.219
52.0	3.037
56.0	2.849
60.0	2.661
64.0	2.474
66.7	2.347

[1]Coordinates are taken from reference 2.

TABLE III.- COORDINATES OF THE NACA 65A009 AIRFOIL

x/c, percent	y/c, percent
0	0
.5	.690
.75	.837
1.25	1.068
2.5	1.463
5.0	1.965
7.5	2.385
10.0	2.736
15.0	3.292
20.0	3.714
25.0	4.034
30.0	4.266
35.0	4.420
40.0	4.495
45.0	4.485
50.0	4.379
55.0	4.173
60.0	3.881
65.0	3.519
70.0	3.099
75.0	2.630
80.0	2.125
85.0	1.601
90.0	1.074
95.0	.547
100.0	.020
L.E. radius 0.00516c	

TABLE IV.- COORDINATES FOR SOLID NACELLE

[Station measured from nacelle nose]

Station, in.	Ordinate, in.
0	0
.100	.070
.330	.169
.830	.336
1.330	.489
1.830	.622
2.330	.747
2.580	.800
2.958	.876
3.585	.974
4.840	1.105
6.095	1.190
7.350	1.240
8.605	1.255
16.830	1.255
17.872	1.237
18.913	1.195
19.955	1.127
20.996	1.029
22.038	.909
23.079	.768
24.121	.616
24.250	.598
Nose radius = 0.05 in.	

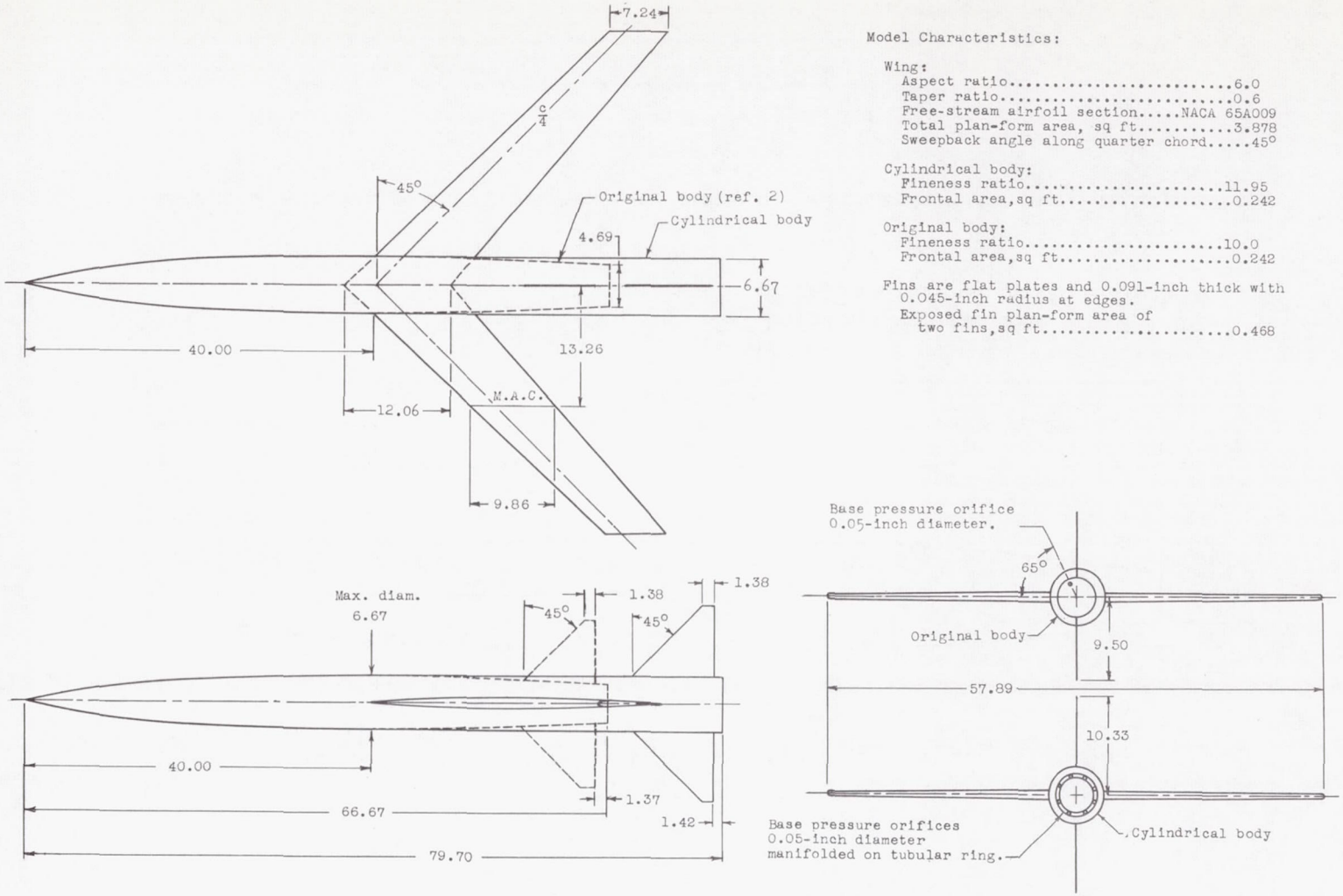

Model Characteristics:

Wing:
- Aspect ratio.....6.0
- Taper ratio.....0.6
- Free-stream airfoil section.....NACA 65A009
- Total plan-form area, sq ft.....3.878
- Sweepback angle along quarter chord.....45°

Cylindrical body:
- Fineness ratio.....11.95
- Frontal area, sq ft.....0.242

Original body:
- Fineness ratio.....10.0
- Frontal area, sq ft.....0.242

Fins are flat plates and 0.091-inch thick with 0.045-inch radius at edges.
- Exposed fin plan-form area of two fins, sq ft.....0.468

Figure 1.- Details and dimensions of the basic wing-body configurations having the cylindrical body and the original body (ref. 2). All dimensions are in inches.

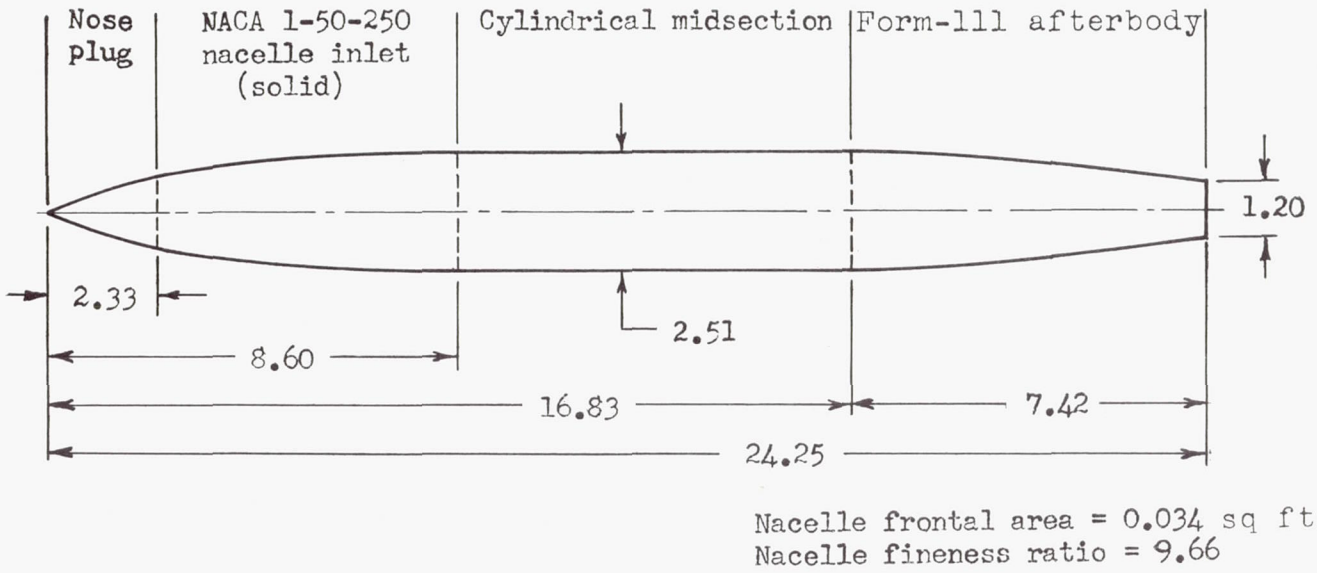

Figure 2.- Details and dimensions of nacelle. All dimensions are in inches.

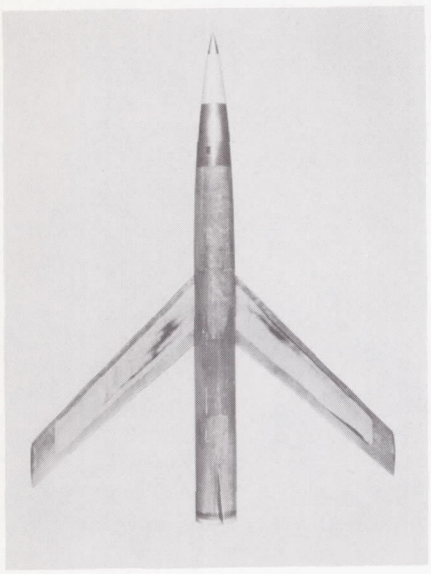

Model A

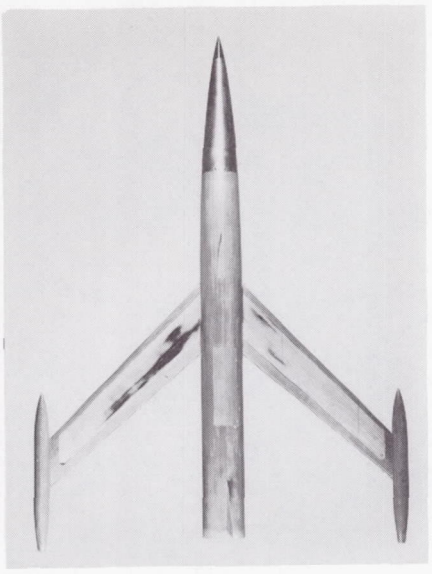

Model B
(nacelles at 0.96b/2)

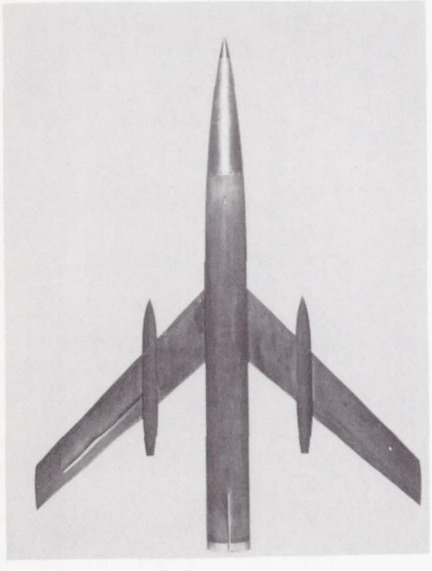

Model C
(nacelles at 0.4b/2)

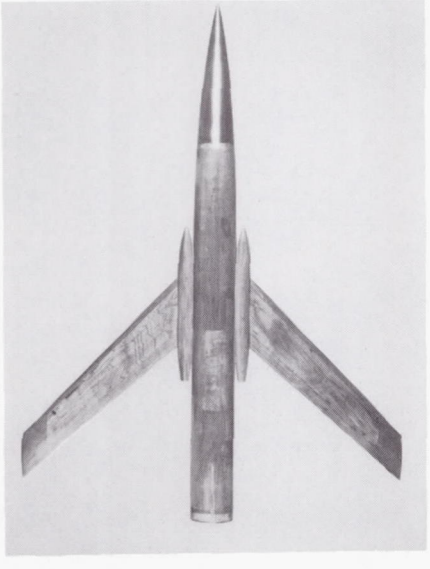

Model D
(nacelles at 0.15b/2)

L-82095

(a) Models with cylindrical body and nacelles in various spanwise positions.

Figure 3.- Photographs of flight models.

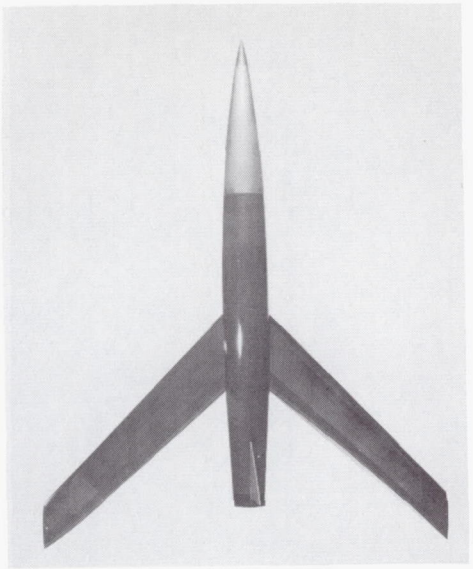

Model E

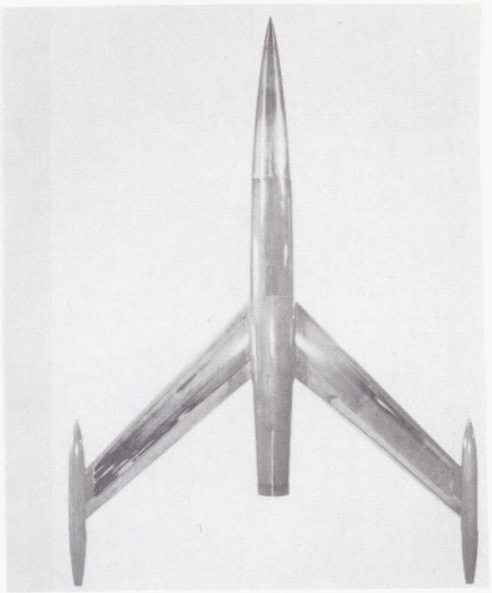

Model F
(nacelles at 0.96b/2)

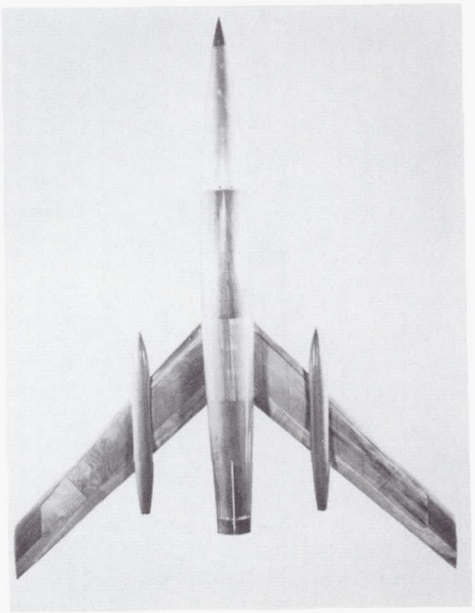

Model G
(nacelles at 0.4b/2)

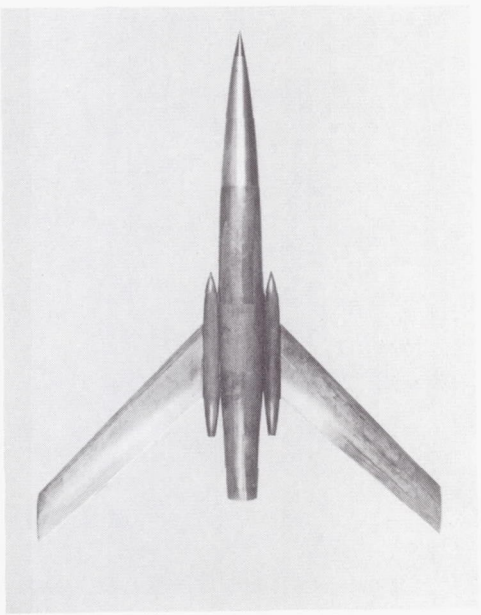

Model H
(nacelles at 0.15b/2)

L-82096

(b) Models with original body and nacelles in various spanwise positions.

Figure 3.- Concluded.

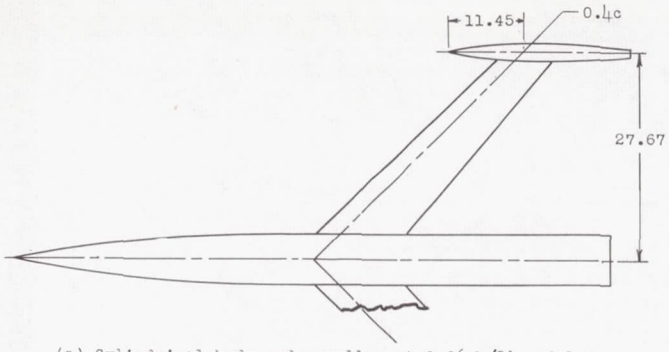

(a) Cylindrical body and nacelles at 0.96 b/2; model B.

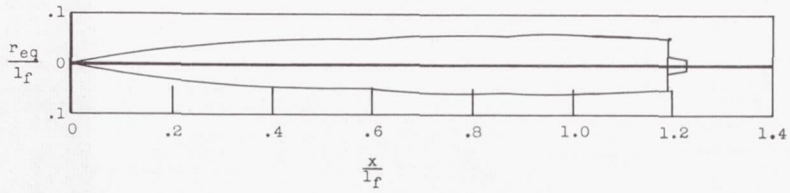

(b) Equivalent body of revolution for model B.

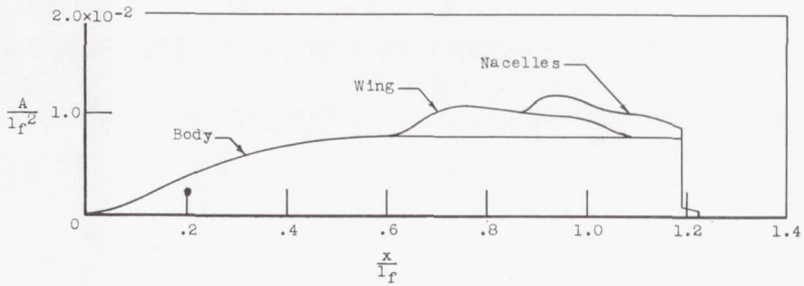

(c) Cross-sectional area distribution for model B.

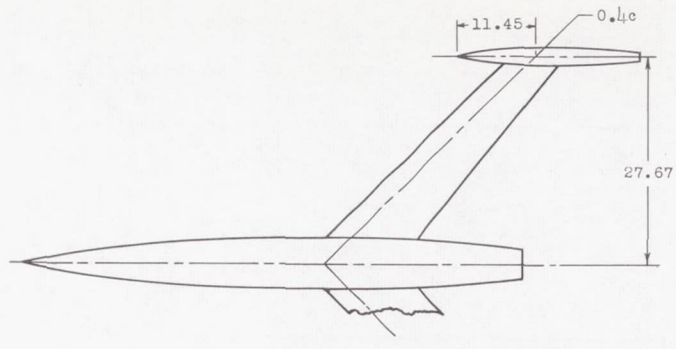

(d) Original body and nacelles at 0.96 b/2; model F.

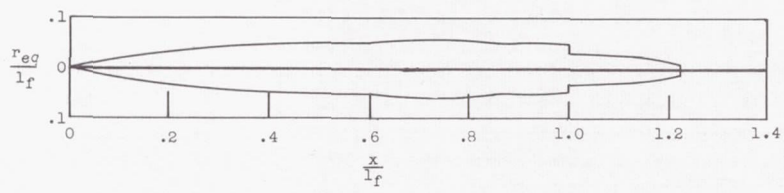

(e) Equivalent body of revolution for model F.

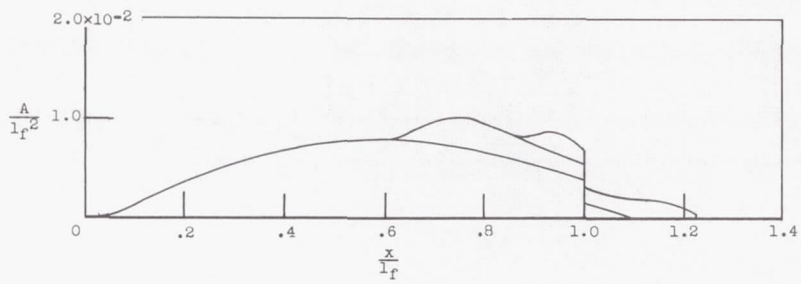

(f) Cross-sectional area distribution for model F.

Figure 4.- Comparison of nacelle location and cross-sectional area distribution of the configurations having the cylindrical body and the original body.

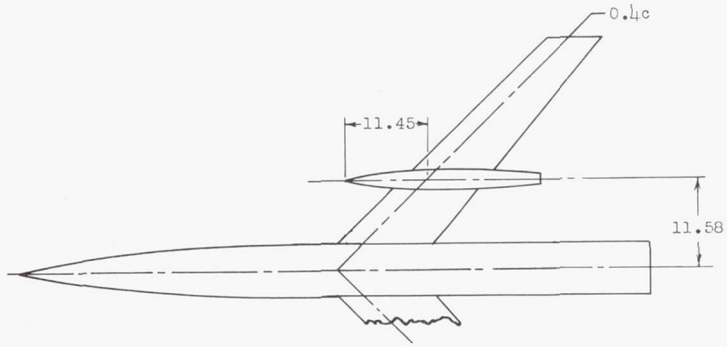

(g) Cylindrical body and nacelles at 0.4 b/2; model C.

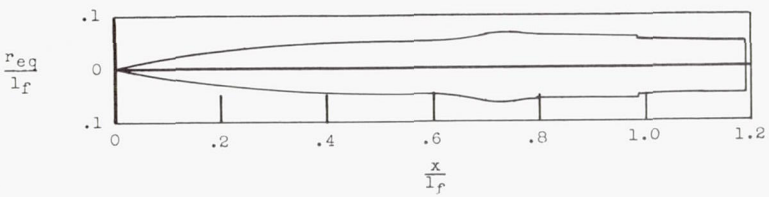

(h) Equivalent body of revolution for model C.

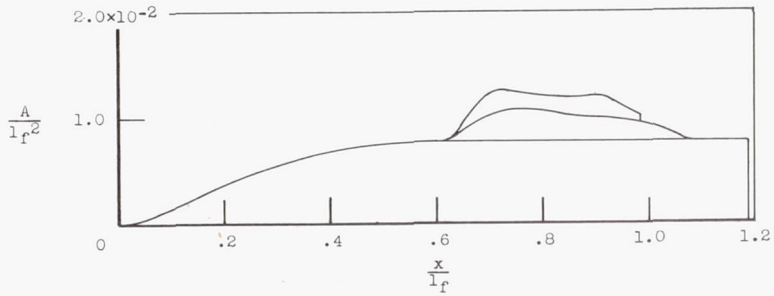

(i) Cross-sectional area distribution of model C.

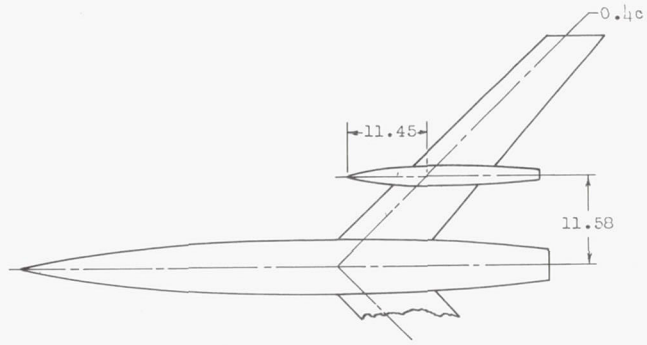

(j) Original body and nacelles at 0.4 b/2; model G.

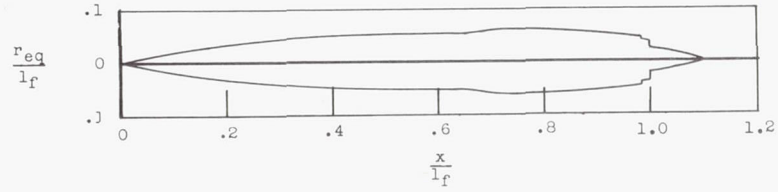

(k) Equivalent body of revolution for model G.

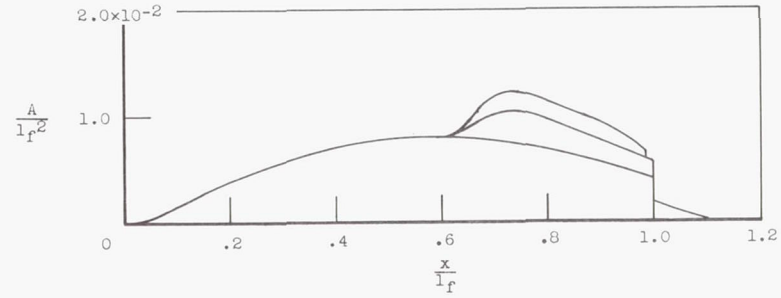

(l) Cross-sectional area distribution for model G.

Figure 4.- Continued.

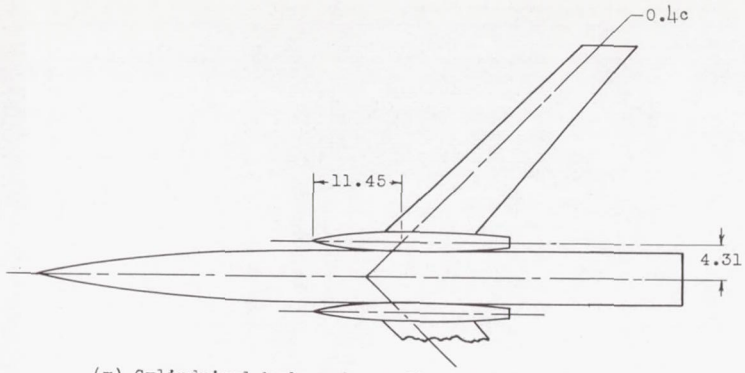

(m) Cylindrical body and nacelles at 0.15 b/2, model D.

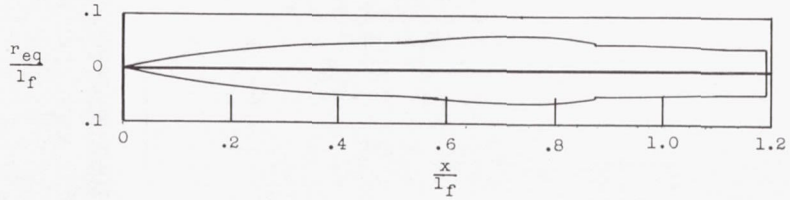

(n) Equivalent body of revolution for model D.

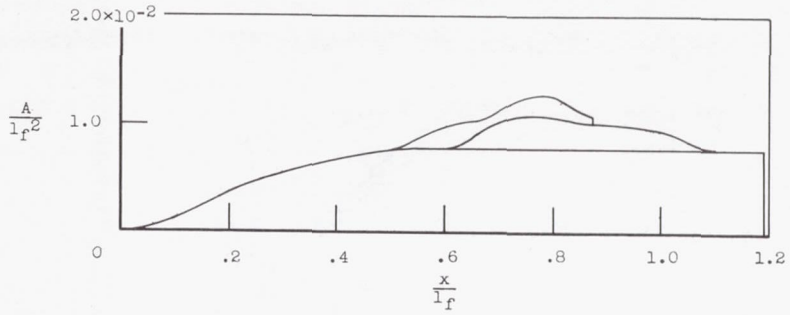

(o) Cross-sectional area distribution for model D.

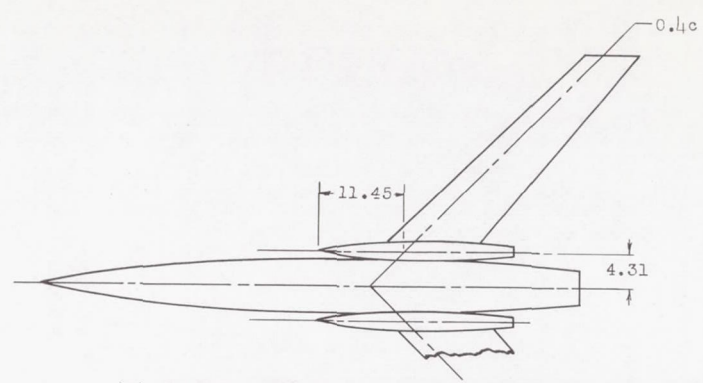

(p) Original body and nacelles at 0.15 b/2, model H.

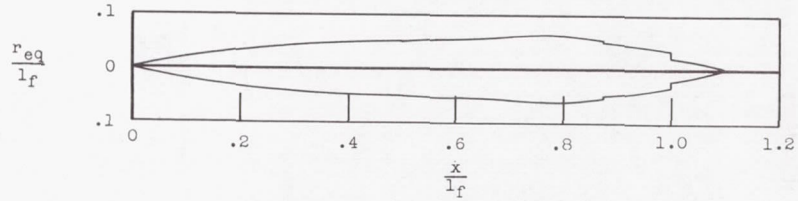

(q) Equivalent body of revolution for model H.

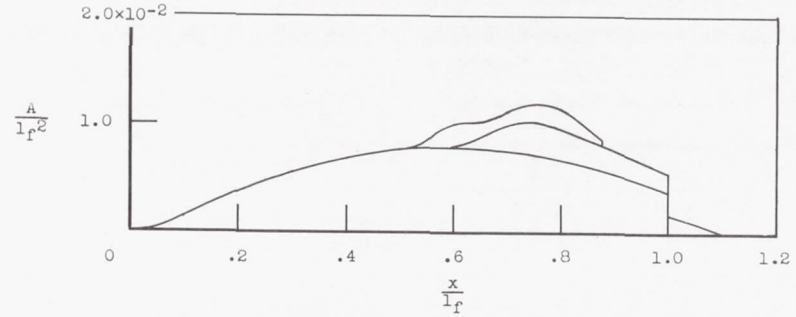

(r) Cross-sectional area distribution for model H.

Figure 4.- Concluded.

L-75962

Figure 5.- Photograph of cylindrical-body configuration and booster on rail launcher.

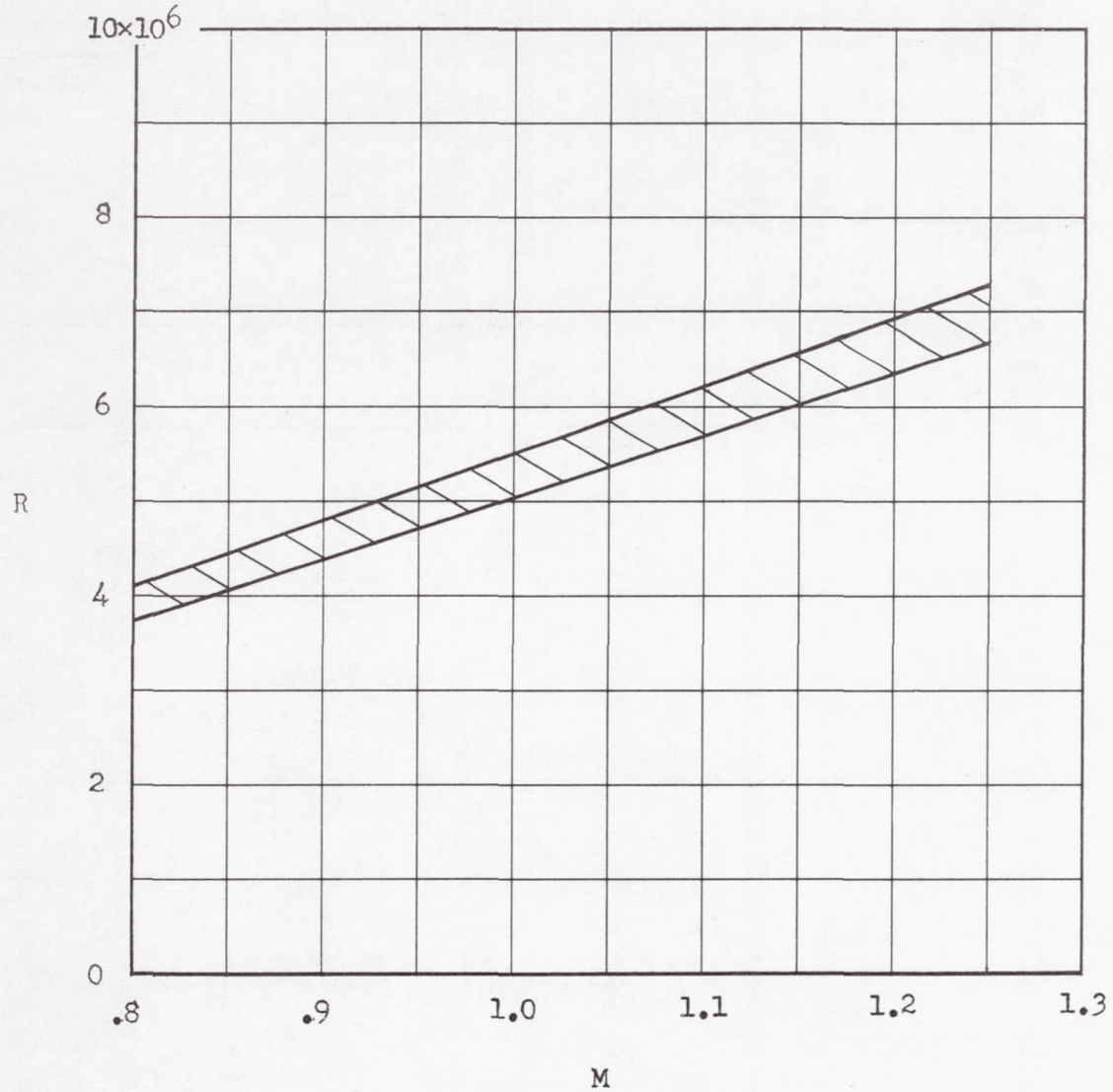

Figure 6.- Variation of Reynolds number with Mach number for models tested. Reynolds number is based on wing mean aerodynamic chord.

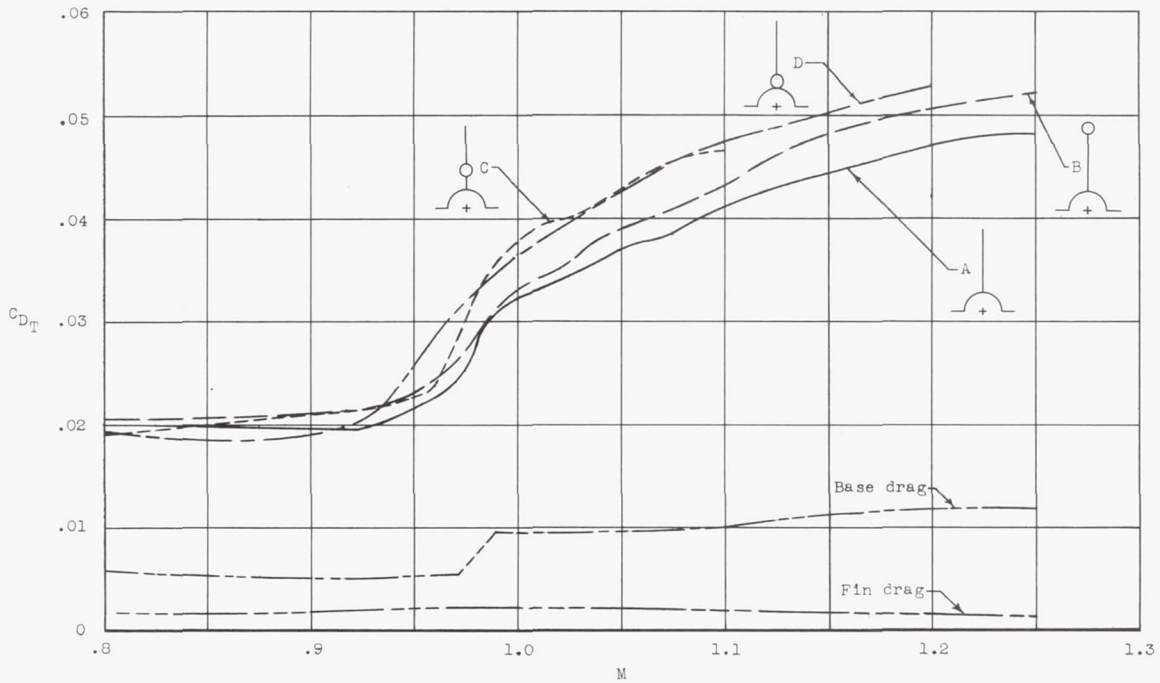

(a) Models with cylindrical fuselage.

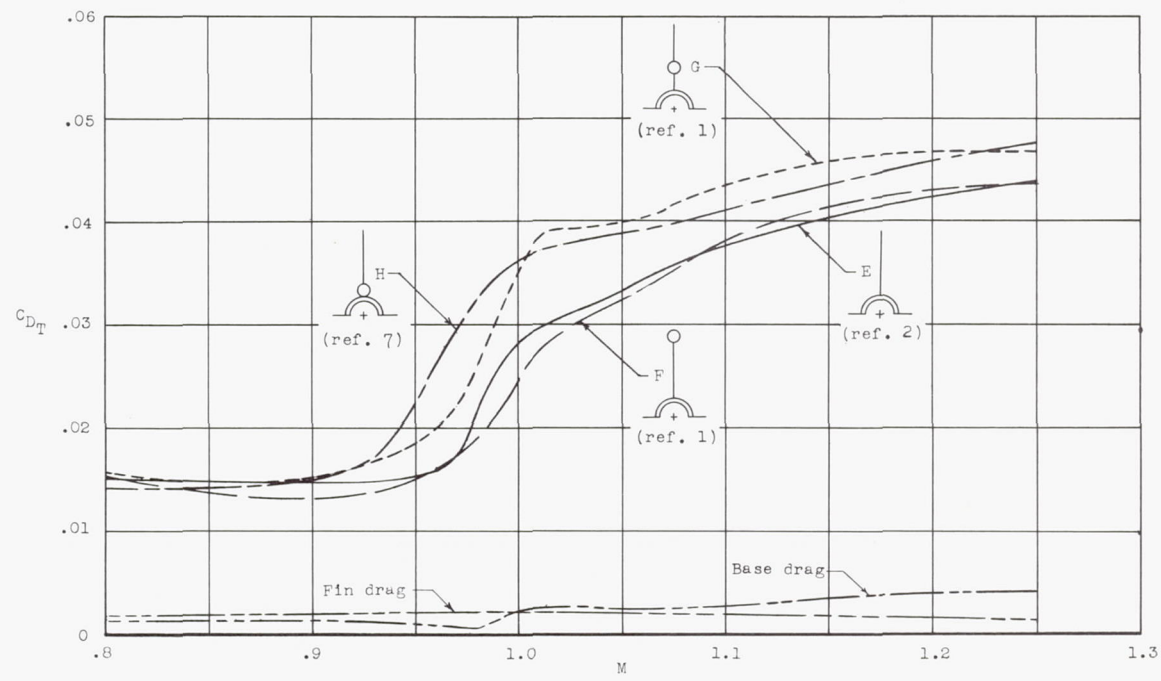

(b) Models with original fuselage.

Figure 7.- Variations of total drag coefficients, base drag coefficients, and fin drag coefficients for the configurations having the cylindrical body and the original body.

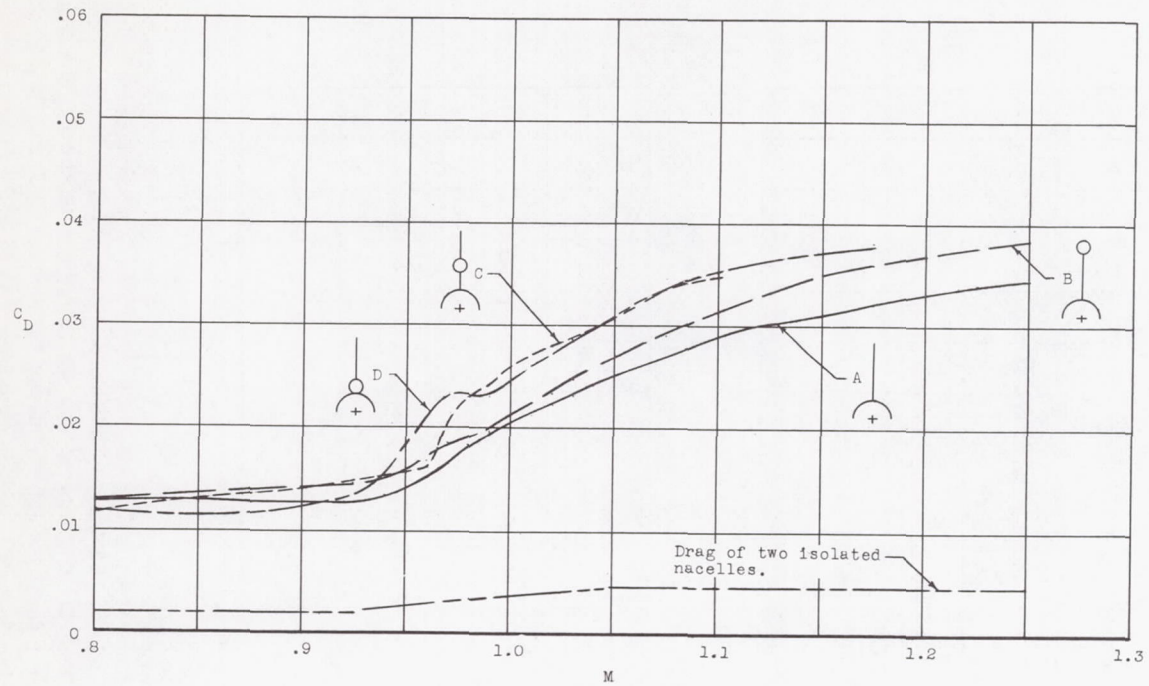

(a) Models with cylindrical fuselage.

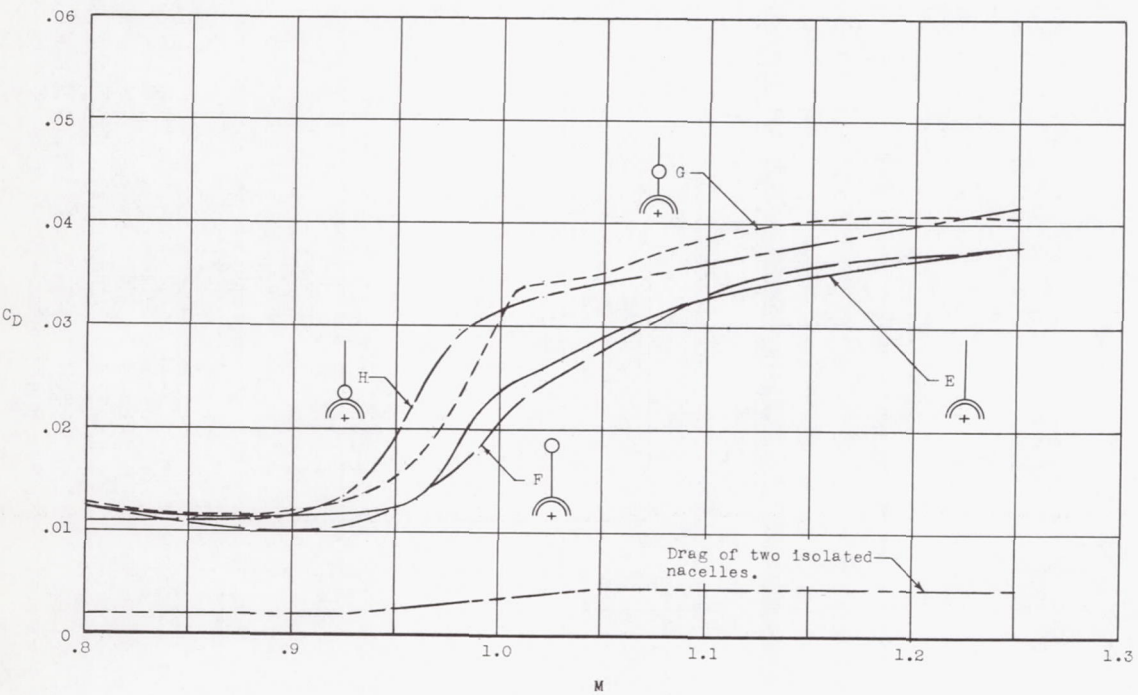

(b) Models with original fuselage.

Figure 8.- Variations of drag coefficient with Mach number for the configurations having the cylindrical body and the original body. Fin drag and base drag coefficients are subtracted.

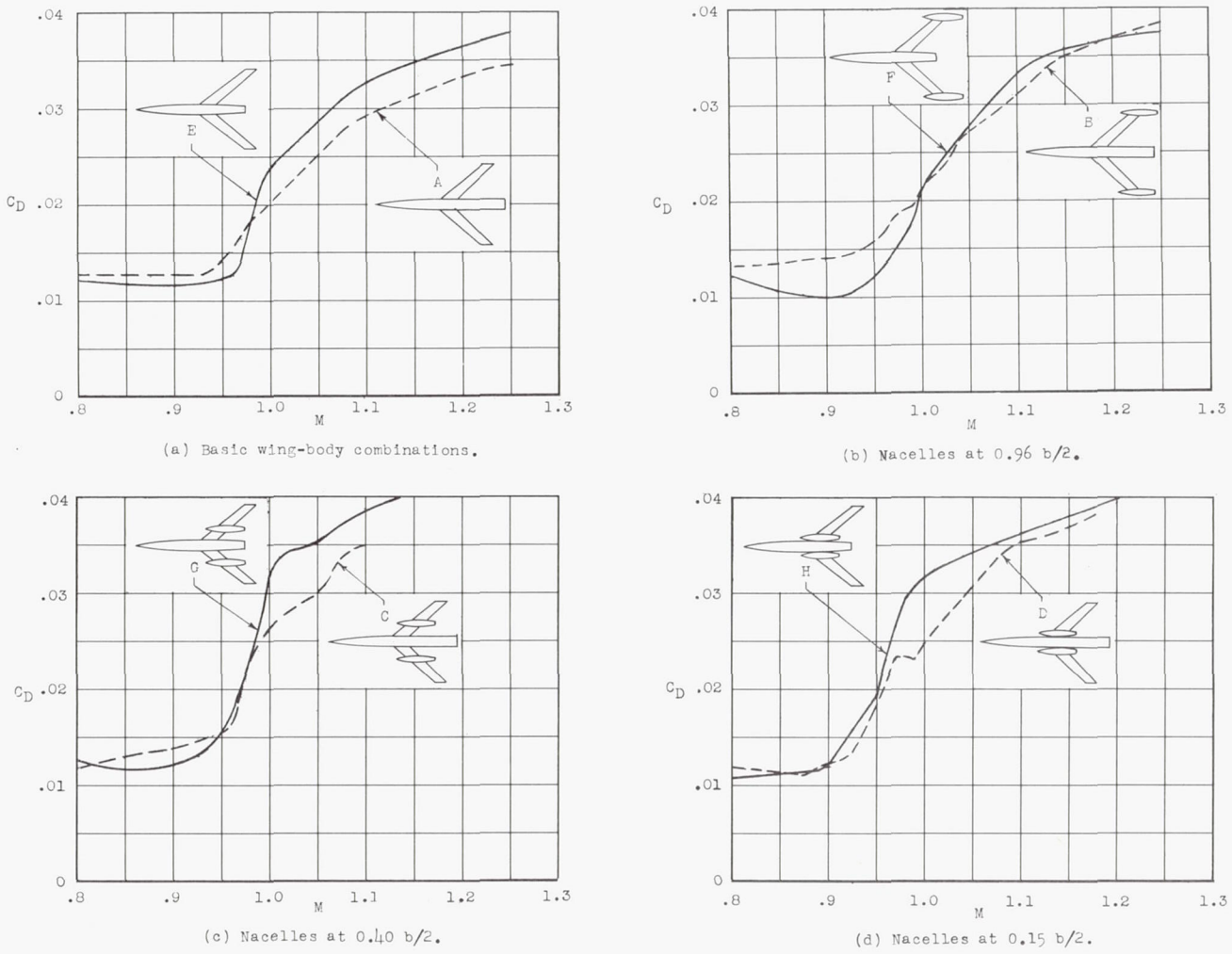

(a) Basic wing-body combinations.

(b) Nacelles at 0.96 b/2.

(c) Nacelles at 0.40 b/2.

(d) Nacelles at 0.15 b/2.

Figure 9.- Comparisons of the effect of afterbody shape on the drag coefficients of the configurations with nacelles at various spanwise locations.

4Y

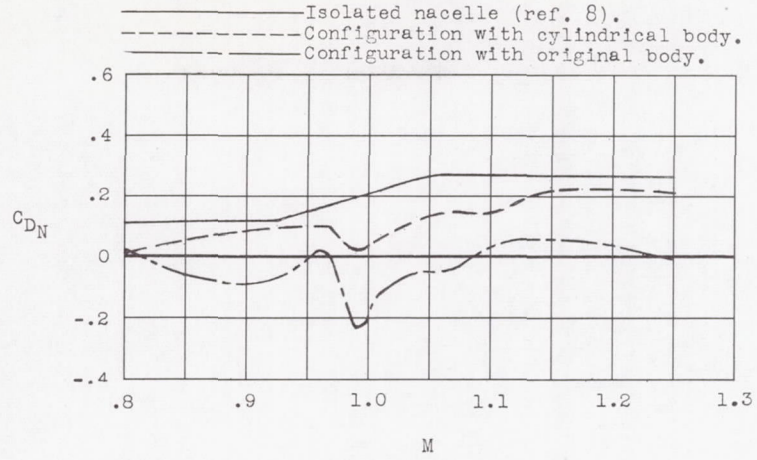

(a) Nacelles at 0.96 b/2.

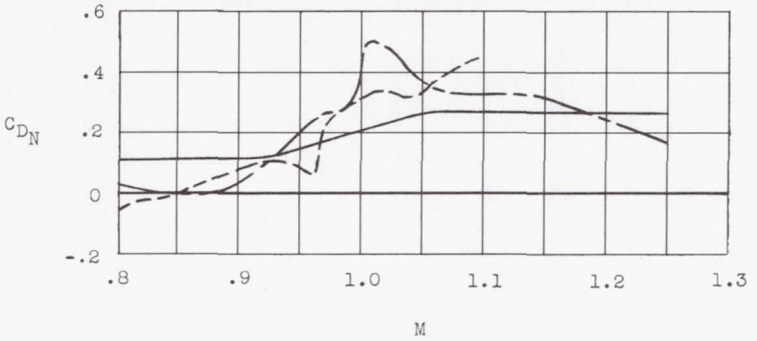

(b) Nacelles at 0.40 b/2.

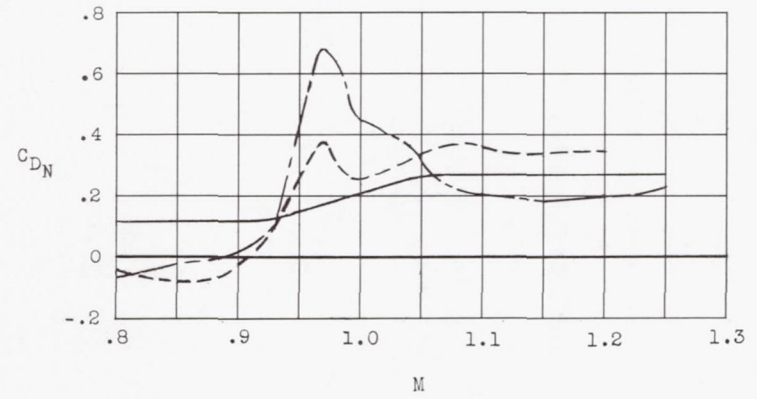

(c) Nacelles at 0.15 b/2.

Figure 10.- Comparisons of the nacelle plus interference drag coefficient for nacelles located in various spanwise positions on the configurations having the cylindrical body and original body.

NACA-Langley - 3-25-54 - 325